

PAPER

## Effect of fuel isotope mass on q-profile formation in JET hybrid plasmas

To cite this article: C.D. Challis *et al* 2020 *Nucl. Fusion* **60** 086008

View the [article online](#) for updates and enhancements.






**IOP | ebooks™**

Bringing together innovative digital publishing with leading authors from the global scientific community.

Start exploring the collection—download the first chapter of every title for free.

# Effect of fuel isotope mass on q-profile formation in JET hybrid plasmas

C.D. Challis<sup>1</sup>, S. Brezinsek<sup>2</sup> , I.H. Coffey<sup>3</sup>, M. Fontana<sup>4</sup> , N.C. Hawkes<sup>1</sup>, D.L. Keeling<sup>1</sup>, D.B. King<sup>1</sup>, G. Pucella<sup>5</sup>, E. Viezzer<sup>6</sup>  and JET Contributors<sup>7</sup>

<sup>1</sup> United Kingdom Atomic Energy Authority, Culham Centre for Fusion Energy, Culham Science Centre, Abingdon, Oxon OX14 3DB, United Kingdom of Great Britain and Northern Ireland

<sup>2</sup> Forschungszentrum Jülich, Institute of Energy and Climate Research – Plasma Physics, TEC, 52425 Jülich, Germany

<sup>3</sup> Astrophysics Research Centre, School of Mathematics and Physics, Queen's University, Belfast BT7 1NN, United Kingdom of Great Britain and Northern Ireland

<sup>4</sup> Ecole Polytechnique Fédérale de Lausanne (EPFL), Swiss Plasma Center (SPC), CH-1015 Lausanne, Switzerland

<sup>5</sup> ENEA, Fusion and Nuclear Safety Department, C.R. Frascati, Via E. Fermi 45, 00044 Frascati (Roma), Italy

<sup>6</sup> Dept. of Atomic, Molecular and Nuclear Physics, University of Seville, Avda. Reina Mercedes, 41012 Seville, Spain

E-mail: [clive.challis@ukaea.uk](mailto:clive.challis@ukaea.uk)

Received 4 February 2020, revised 28 April 2020

Accepted for publication 20 May 2020

Published 10 July 2020



CrossMark

## Abstract

The initial current ramp phase of JET hybrid plasmas is used to optimise the target q-profile for main heating to allow access to high  $\beta$  and avoid MHD instabilities. Mixed protium-deuterium experiments, carried out at JET since the installation of the beryllium-tungsten wall, have shown that the q-profile evolution during this Ohmic phase varies systematically with average main ion isotope mass, indicating the need for re-optimisation for future T and mixed D-T experiments. Current diffusion modelling shows that the key factor was a reduction in electron temperature profile peaking as the hydrogenic isotope mass was increased. This was correlated with an increase in plasma radiation by metallic impurities, consistent with the increased sputtering yield by higher mass isotopes during the current ramp phase. Reduced electron temperature peaking can lead to magnetic shear reversal and the appearance of a 2/1 mode, which can lock, causing the JET massive gas injection system to be triggered to avoid an unmitigated disruption. The potential for a further reduction in electron temperature peaking in T and D-T plasmas could, therefore, result in an increased risk of disruptions. To mitigate this risk, electron temperature peaking measurements have been included in the real-time control system to allow this type of disruption to be avoided by central heating, density increase or early pulse termination. These experiments indicate the need for integrated modelling of impurity behaviour, including the plasma core, scrape-off layer and plasma wall interactions, to predict q-profile evolution in the current ramp phase and anticipate the effects of isotope changes.

Keywords: isotope, q-profile, JET, tokamak

(Some figures may appear in colour only in the online journal)

<sup>7</sup> See Joffrin et al 2019 ([10.1088/1741-4326/ab2276](https://doi.org/10.1088/1741-4326/ab2276)) for the JET team.

## 1. Introduction

The sensitivity of core transport and MHD instabilities to the  $q$ -profile shape in tokamak plasmas has led to the use of plasma current profile optimisation as a technique to develop plasmas with high fusion performance. This approach has been used in the development of hybrid plasmas, where access to improved confinement with respect to the IPB98(y,2) scaling [1] at high normalised  $\beta$  ( $\beta_N = \beta_T a B_T/I_P$ ) generally relies on the generation of a  $q$ -profile with a wide region of low magnetic shear at, or slightly above,  $q = 1$  in the plasma core [2–4]. The JET hybrid plasma scenario is being developed for use in future experiments with pure tritium (T) and mixed deuterium-tritium (D-T) fuel [5]. In this scenario the current profile shape is optimised using the initial Ohmic current ramp phase such that the desired  $q$ -profile shape is achieved at the start of the main heating pulse. The restriction on the amount of tritium that can be used at JET and the total number of 14 MeV neutrons that can be produced mean that the number of T and D-T pulses will be strictly limited, and relatively little experimental time can be devoted to re-optimising the scenario to compensate for isotope dependent changes. Therefore, in preparation for the future T and D-T experiments, it is necessary to understand the effect of the main ion isotope mass on the evolution of the  $q$ -profile in the Ohmic ramp phase to anticipate changes in plasma behaviour and identify techniques to mitigate any detrimental impact on plasma fusion performance. Although some relevant experience was gained in previous JET D-T experiments, these were performed in the presence of a carbon first wall (JET-C). The next D-T experiments will be carried out with the JET ITER-like wall (JET-ILW), comprised of tungsten and tungsten coated plasma facing components in the divertor and a dominantly beryllium first wall in the main chamber, which results in different plasma impurity composition that can affect the  $q$ -profile evolution in the current ramp phase.

Several factors could result in changes in the  $q$ -profile evolution during the Ohmic ramp phase of tokamak plasmas when the hydrogenic isotope mass is varied. Some early empirical energy confinement scalings (e.g. [6]) showed a tendency for confinement to increase with hydrogenic isotope mass in Ohmically heated plasmas. This is consistent with many Ohmic experiments on individual tokamaks that have shown higher energy confinement in deuterium plasmas compared with protium [7]. Recent Ohmic JET-ILW experiments showed higher electron temperature in deuterium plasmas compared with similar protium experiments, which was due to increased energy confinement and reduced electron-ion coupling in the deuterium case [8]. Experiments on ASDEX have also shown increased impurity content in Ohmic deuterium plasmas compared with protium [7] and central impurity accumulation was reported in Ohmic deuterium plasmas in ISX-B, but not in protium plasmas [9]. At this point it should be noted that the sputtering yield for metallic impurities tends to increase with isotope mass for hydrogenic species. In the case of JET-ILW plasmas this can result in an increased source of beryllium [10], which, in turn, further enhances the sputtering of high  $Z$  impurities from the W divertor [11]. In the

case of lower  $Z$  impurities, this can result in an increase in the effective  $Z$  of the plasma, whereas the increase in higher  $Z$  impurities can also lead to increased plasma radiation in the confined region and a reduction in the electron temperature. The variations in the magnitude and radial profile of both the electron temperature and  $Z$ -effective in the confined plasma directly affect the plasma resistivity, thereby affecting the rate of current diffusion during the Ohmic ramp phase and the  $q$ -profile produced at the start of the main heating pulse.

Hybrid plasmas have never been operated in T or D-T. However, JET-C experiments with internal transport barriers (ITBs) that were sensitive to the  $q$ -profile shape were carried out in the 1997 D-T campaign [12]. These relied on the formation of a  $q$ -profile with a  $q = 2$  magnetic surface in the core region of the plasma. It was reported that the  $q$ -profiles produced in D-T experiments were slightly different from reference deuterium plasmas, and modifications were needed to the heating power waveform and the start time of the high power heating pulse to obtain similar ITBs to the reference D experiments. With this experience in mind, experiments carried out since the installation of the JET-ILW wall with mixed protium and deuterium plasmas have been studied to investigate the effect of the isotope mass on the initial  $q$ -profile evolution. A series of pulses were obtained using an Ohmic current ramp phase with similar characteristics to the JET hybrid scenario. The average main ion mass number was scanned between 1 and 2 in otherwise similar conditions, allowing the effect of the isotope mass to be studied.

In this paper, the observed effect of varying the hydrogenic isotope mass on the  $q$ -profile evolution during the Ohmic ramp phase is shown for conditions relevant to the JET-ILW hybrid scenario. The key plasma parameters that correlate with this effect are identified and the results of current diffusion modelling are presented, allowing the causes of the change in  $q$ -profile evolution to be identified. The implications of the results for future T and D-T operation are discussed, and potential strategies to mitigate the effects of changing the main ion isotope mass are proposed. Finally, the work is summarised and conclusions are drawn. An initial conference presentation of this work was made at [13].

## 2. Protium-deuterium mixture scan experiment

JET-ILW experiments have been performed using mixed protium-deuterium plasmas to scan the main ion isotope mass [14]. The time evolution of the current ramp phase of a typical plasma is illustrated in figure 1. The pulse exhibits the characteristic features of a JET hybrid plasma, including: (1) the rapid development of a large volume plasma and early transition from the limiter to an X-point plasma, which minimises the rate of current diffusion towards the plasma centre during the main current ramp-up phase [15]; (2) low density during the Ohmic phase to maintain a relatively high electron temperature to further slow the current diffusion; and (3) a current ‘overshoot’ before the start of the main heating pulse, which produces a wide region of low core magnetic shear with a high shear region near the plasma edge. After

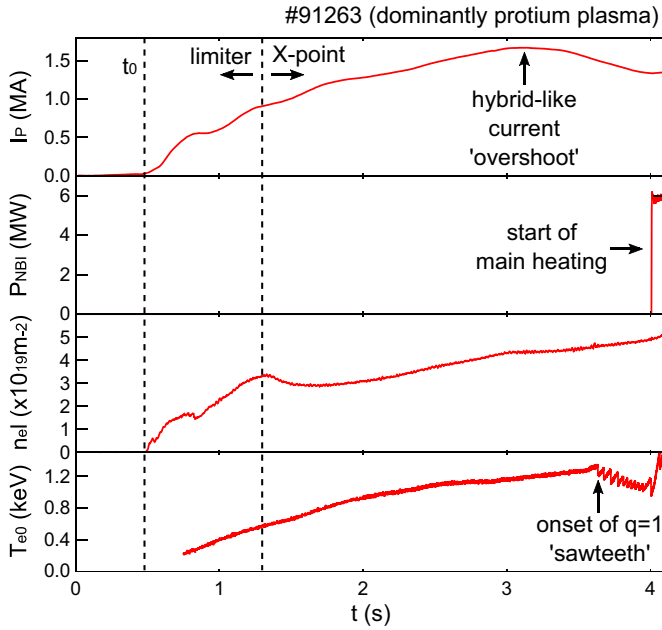


**Figure 1.** Time evolution of plasma current, neutral beam injection heating power, plasma density and central electron temperature during the initial current ramp phase of a typical plasma from the protium-deuterium mixture scan. The vertical lines indicate the time of plasma initiation ( $t_0$ ) and transition from limiter to X-point, respectively. The time of the first  $q = 1$  sawtooth crash is also indicated.

the current ‘overshoot’, when  $q_0$  is close to 1, high power heating is typically applied in hybrid experiments to generate a high  $\beta_N$  plasma. In the mixed protium-deuterium experiments described in this paper the magnetic field strength was  $\approx 1.7$  T and the plasma current became steady at  $\approx 1.4$  MA at the start of the main neutral beam injection (NBI) heating pulse. Relatively low power was applied in these experiments due to a limitation on the protium NBI power available, which effectively constrained the power level throughout the scan to maintain comparable conditions. The JET-ILW hybrid plasma scenario is also being developed with higher heating power, plasma current and magnetic field to achieve high fusion power in future D-T experiments [5]. The method used to optimise the  $q$ -profile shape is similar for the high fusion performance plasmas and the protium-deuterium experiments. Consequently, the investigation presented in this paper provides a basis for anticipating the impact of adding tritium in such plasmas, allowing mitigation strategies to be prepared in advance of the next T and D-T experiments.

To avoid the risk that long timescale variations in the conditions inside JET (e.g. impurity contamination on plasma facing component surfaces) might affect the  $q$ -profile evolution and complicate the analysis of the main ion isotope mass effect, the dataset used for the analysis presented in this paper was restricted to plasmas of the type shown in figure 1 that were obtained during a single week of plasma operation. Plasma density variations can also affect the  $q$ -profile evolution in the current ramp phase, so the analysis dataset was further restricted to plasmas with similar density during the Ohmic

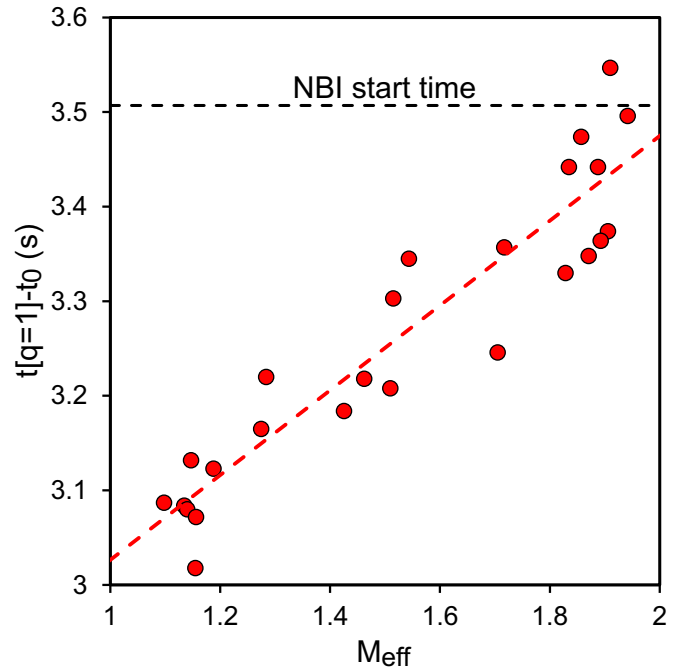


**Figure 2.** Onset time of MHD activity associated with  $q = 1$  relative to the time of plasma initiation plotted against the effective main ion isotope mass (averaged over  $t = 1.5$ – $3.5$  s). A linear fit to the data is shown and the start time of the NBI heating pulses is illustrated.

X-point phase. The overall variation in volume averaged density, averaged over the period  $t = 1.5$ – $3.5$  s, was less than 10%. Finally, one pulse was deselected due to an impurity influx close to the time of X-point formation, which led to an abrupt increase in plasma radiation. The type of plasma illustrated in figure 1 was designed to achieve  $q_0 \approx 1$  at the start of the main heating when using deuterium gas injection. No attempt was made to re-optimize the  $q$ -profile as the main ion isotope mass was varied.

It can be seen in figure 1 that 1/1 MHD activity is observed in the form of electron temperature sawteeth shortly before the start of the NBI heating pulse. The first sawtooth crash is typically preceded by a slow oscillation on the electron temperature measurements in the plasma core, which we have taken to provide an indication of the relative arrival time of the  $q = 1$  magnetic surface in the plasma for the pulses in this dataset. Figure 2 shows the onset time of the slow oscillation, estimated visually using ECE measurements, relative to the time of plasma initiation (shown as  $t_0$  in figure 1) plotted against the effective main ion isotope mass number ( $M_{\text{eff}} = 2 - n_p / [n_p + n_D]$ , where  $n_p$  is the protium density and  $n_D$  is the deuterium density).  $M_{\text{eff}}$  was determined from visible spectroscopy measurements using a line-of-sight that passes through the outer divertor region. This measurement indicates the isotope ratio of the particles recycled at the wall and the injected gas. However, this value has previously been found to be representative of the isotope mixture in the plasma core for unfuelled Ohmic plasmas in JET-C [16] and even NBI heated plasmas in JET-ILW where the injected isotope ratio is steady [14, 17]. It should be noted that, due to the low values of the

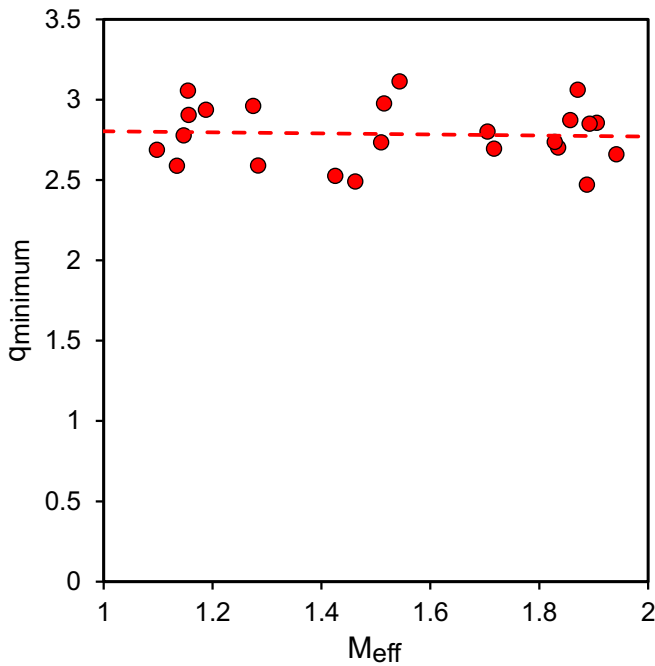


**Figure 3.** Minimum value of  $q$  at the start of the X-point phase (averaged over  $t = 1.25$ – $1.75$  s) plotted against the effective main ion isotope mass (averaged over  $t = 1.5$ – $3.5$  s). A linear fit to the data is shown.

effective ion charge ( $Z_{\text{eff}}$ ) in these plasmas, the evaluation of the total effective ion mass, including impurities, gives similar values to the main ion definition of  $M_{\text{eff}}$  above. The data in figure 2 indicate that the arrival time of the  $q = 1$  magnetic surface was progressively delayed as  $M_{\text{eff}}$  was increased from 1 to 2.

The  $q$ -profile has been evaluated for all but two of the plasmas in the dataset using EFIT [18] equilibrium reconstructions constrained by plasma pressure and polarimetry measurements. Figure 3 shows the minimum value of  $q$  for each pulse at the start of the X-point phase plotted against  $M_{\text{eff}}$ . As there are very few measurements of  $M_{\text{eff}}$  during the averaging period used for the  $q$ -profile measurements, the  $M_{\text{eff}}$  data was averaged over the same period as for figure 2. Although there is significant scatter between the  $q$  measurements shown in figure 3, no clear trend is observed with the main ion isotope mass, despite that fact that some parameters, such as beryllium line emission, exhibited systematic variations with main ion isotope mass during the limiter phase. The results shown in figure 3, therefore, suggest that changes in the current diffusion during the X-point phase were the main cause of the variation in the  $q$ -profile at the start of the main heating pulse illustrated in figure 2.

A key factor that affects the diffusion of current into the core of a tokamak plasma during the Ohmic ramp phase is the plasma resistivity. In general, the higher the plasma resistivity, the faster the rate of current diffusion. Spitzer resistivity [19] has no specific plasma ion mass dependence, but increases with  $Z_{\text{eff}}$  and decreases with increasing electron temperature. Figure 4 shows the volume average electron temperature,

measured using an ECE Michelson interferometer [20], and  $Z_{\text{eff}}$ , determined from visible bremsstrahlung measurements [21], plotted as a function of  $M_{\text{eff}}$  for the plasmas illustrated in figure 2. The ECE spectra were mapped to the equilibrium flux surfaces using an improved toroidal magnetic field determination based on optical fibre coil current measurements [22]. The  $Z_{\text{eff}}$  measurements were made using a vertical chord through the plasma at a major radius that is larger than the typical magnetic axis location, such that it excludes the plasma within  $r/a \approx 0.3$ . This means that the measurement is not sensitive to the central impurity concentration, but is, instead, representative of the region outside the plasma centre, through which the current diffuses during the current ramp phase.

It can be seen from figure 4 that the plasma electron temperature increased with main ion isotope mass, which is consistent with Ohmic experiments performed during the stationary plasma current phase [8]. Although this might be expected to lead to a reduction in plasma resistivity as  $M_{\text{eff}}$  increases, the effect was counteracted by a collinear increase in the effective ion charge, as illustrated in figure 4. Current diffusion modelling, presented in the next section, confirms that the changes in the average electron temperature and  $Z_{\text{eff}}$  compensate each other such that, together, they do not explain the observed change in  $q$ -profile evolution as  $M_{\text{eff}}$  was varied.

The increase in  $Z_{\text{eff}}$  indicates an increase in plasma impurity concentration as the main ion isotope mass was increased. This is confirmed by a substantial increase in bulk plasma radiation with  $M_{\text{eff}}$ , shown using bolometer camera [23] measurements in figure 5. The bulk radiation was estimated using the low field side channels of the vertical camera assuming poloidal symmetry, which is a reasonable assumption for these Ohmic plasmas that have low toroidal rotation. Data from the high field side channels were not used because channels close to, or slightly to the high field side of, the magnetic axis also include radiation associated with the divertor. However, signals from peripheral high field side channels show a similar trend of radiation increasing with  $M_{\text{eff}}$ . JET is also equipped with a lateral bolometer camera, which is mounted on the tokamak at a different toroidal location. The data from this camera were not included in figure 5 due to signal pollution in the case of protium gas injection, which was typically from a gas valve at a similar toroidal location as the camera. The gas valves used for protium and deuterium gas injection for the vast majority of the plasmas shown in figure 5 were equidistant from the vertical camera location, making this the ideal instrument to assess the change in power radiated from within the confined plasma as  $M_{\text{eff}}$  was varied. Nevertheless, it will be shown below that the lateral camera data is consistent with an increase in bulk plasma radiation with main ion isotope mass when comparing specific protium and deuterium plasmas where localised gas injection close to the camera was avoided.

Spectroscopic measurements show that the emission from spectral lines associated with many impurities (including Be, O, Fe, Ni, Cu) increased with main ion isotope mass, particularly during the diverted phase of the current ramp. The variation in emission from a Be II line and a Ni XVIII line with  $M_{\text{eff}}$  are shown in figure 6. The Be II line, measured using visible spectroscopy, and the Ni XVIII line, measured using



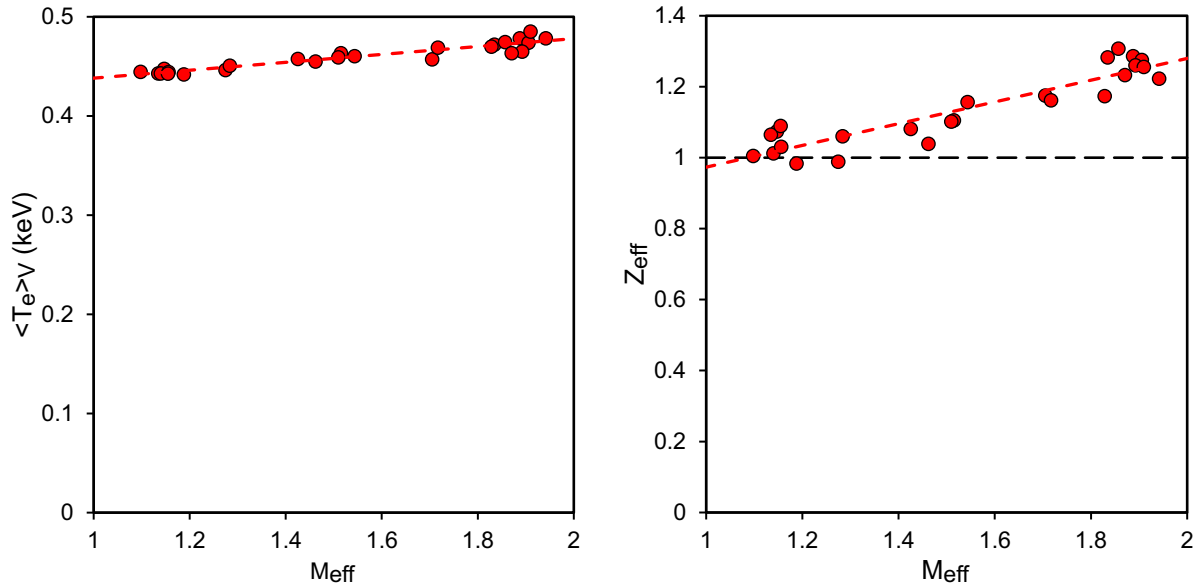


**Figure 4.** Volume averaged electron temperature (left) and  $Z_{\text{eff}}$  (right) plotted against the effective main ion isotope mass. All measurements averaged over  $t = 1.5\text{--}3.5$  s. Linear fits to the data are shown. A line at  $Z_{\text{eff}} = 1$  (dashed black) indicates the level for a pure hydrogenic plasma.

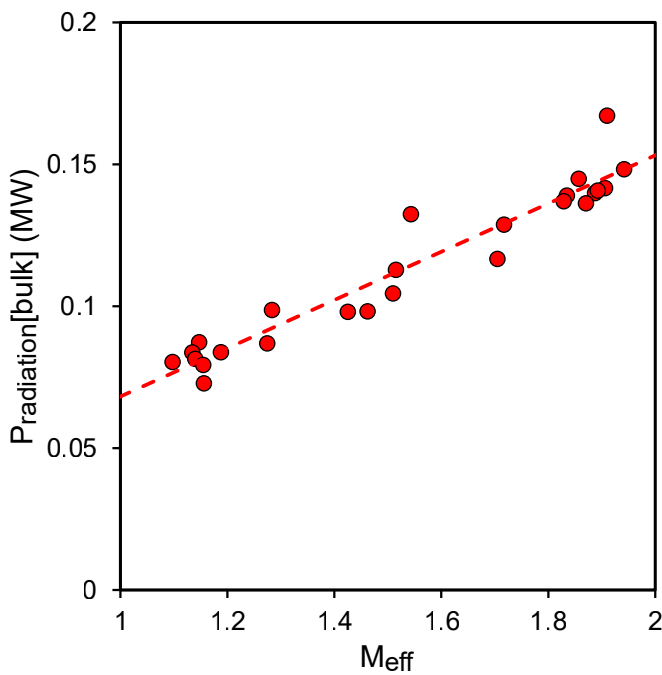


**Figure 5.** Bulk plasma radiation plotted against the effective main ion isotope mass. All measurements averaged over  $t = 1.5\text{--}3.5$  s. A linear fit to the data is shown.

VUV spectroscopy, are indicative of conditions outside and inside the confined plasma, respectively. Both measurements were made using horizontal lines-of-sight through the plasma core. Given the relatively small variation in plasma density and electron temperature throughout this experimental dataset, the systematic changes in impurity line emission is evidence of an increased metallic impurity concentration as  $M_{\text{eff}}$  was

increased. The increase in beryllium concentration is consistent with the increase in sputtering yield by roughly a factor of two for deuterium compared with protium [10]. The spectroscopic analysis of tungsten emission is inconclusive due to the high density of impurity lines in the VUV spectrum. However, the increased beryllium concentration is expected to increase tungsten sputtering in the divertor for such plasmas [11]. The source of impurities such as nickel is more complex. The main source is sputtering from Inconel surfaces in recessed locations by neutral particles from charge-exchange processes [24]. However, other sources may now exist due to Ni migration to other locations. Nevertheless, the source of such impurities is expected to increase with main ion isotope mass, whether it is due to the increased sputtering yield by hydrogenic isotopes or by the increased beryllium concentration in the plasma. In addition to the mass dependence of impurity sputtering yield, any mass dependence of impurity transport within the plasma would also contribute to the effects described in this paper. There are no direct measurements of impurity transport for these plasmas, but findings have been reported from comparisons of deuterium with protium and/or helium plasmas in various tokamaks ranging from impurity transport or confinement that did not vary significantly for main ions of different mass (e.g. [25, 26]) to an approximately linear dependence of impurity confinement time with main ion mass (e.g. [27]). The possibility cannot be ruled out, therefore, that impurity transport effects also contributed to the strong increase in the Ni XVIII signal with  $M_{\text{eff}}$  indicated in figure 6. The observed increase in a wide range of impurities in the plasma provides the explanation for the increases in both  $Z_{\text{eff}}$  and bulk plasma radiation.

There is evidence that the increase in bulk plasma radiation with  $M_{\text{eff}}$  was accompanied by an increase in radiation peaking at the centre of the plasma, which increased during the

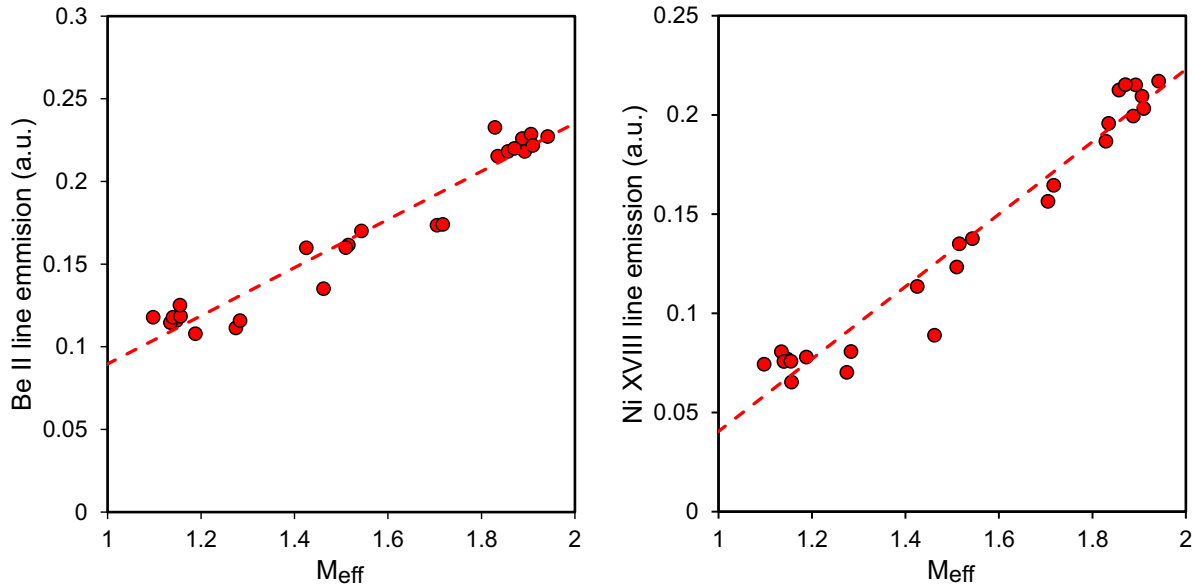


**Figure 6.** Emission measured for Be II (left) and Ni XVIII (right) spectral lines, measured using visible and VUV spectroscopy, respectively, plotted against the effective main ion isotope mass. All measurements averaged over  $t = 1.5\text{--}3.5$  s. Linear fits to the data are shown.

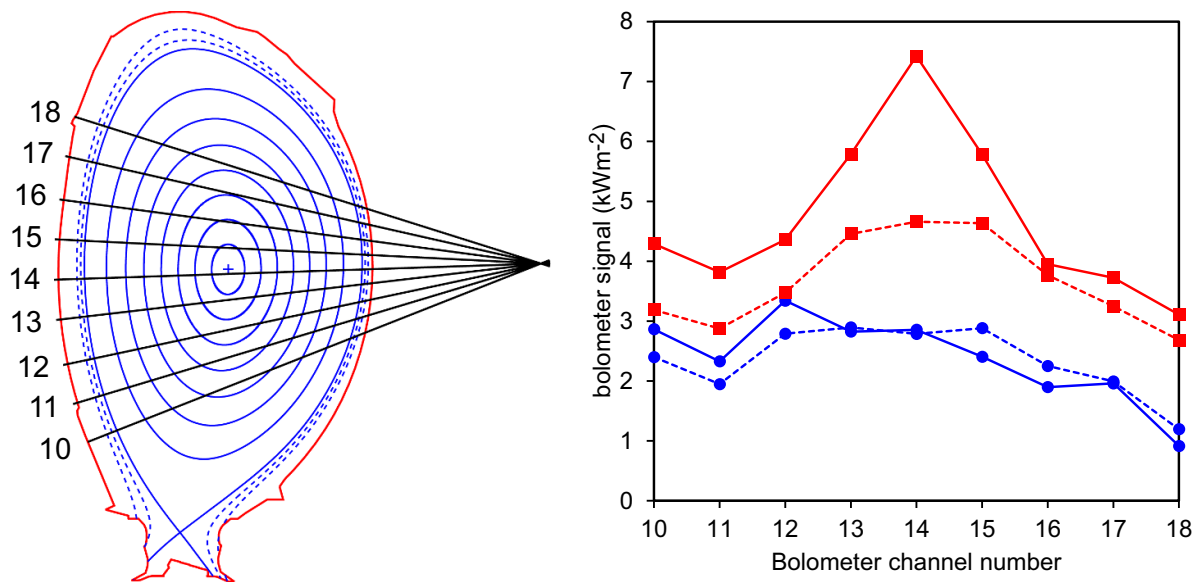


**Figure 7.** Illustration of the most central lines-of-sight of the lateral bolometer camera with plasma flux surfaces for pulse #91276 at  $t = 2.5$  s (left). Bolometer signal versus channel number for a dominantly protium plasma (#91276—blue circles) and a dominantly deuterium plasma (#91226—red squares) (right). Dashed lines show data averaged over  $t = 1.5\text{--}2.5$  s and solid lines show data averaged over  $t = 2.5\text{--}3.5$  s. The pre-pulse baseline signal has been subtracted in all cases.

X-point phase. A systematic analysis of the radiation peaking is not possible as the protium gas was typically injected using a gas valve located at the top of the JET vessel, close to the toroidal location of the lateral bolometer camera. This resulted in pollution of the bolometer signals by radiation originating from outside the separatrix. However, for one of the dominantly protium plasmas (#91276), the gas was injected from a toroidally distributed location in the divertor. The bolometer signals from this pulse have been compared with a dominantly deuterium plasma (#91226) with gas injection from a valve at

the top of the vessel, but far from the lateral bolometer camera location. Although the possibility of some signal contamination by gas cannot be completely ruled out in these cases, the effect is small enough that details of the radiation profile near the centre of the plasma can be seen. The lines-of-sight of the most central channels of the bolometer camera are illustrated in figure 7 along with the signals obtained during these two pulses. The overall increase in the bolometer signals for the dominantly deuterium plasma compared with the dominantly protium plasma is consistent with the increase in bulk

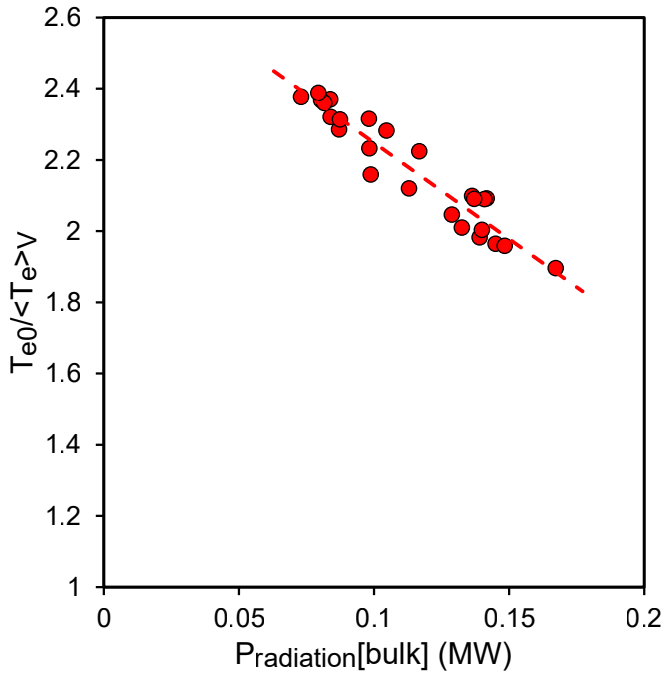


**Figure 8.** Electron temperature peaking plotted against bulk plasma radiation. All measurements averaged over  $t = 1.5\text{--}3.5$  s. A linear fit to the data is shown.

plasma radiation with  $M_{\text{eff}}$  seen in figure 5. Radiation peaking can be seen in the case of the dominantly deuterium plasma in figure 7, centring on channel 14, which passes close to the plasma magnetic axis. This feature, which is not seen in the dominantly protium plasma, is most evident towards the end of the Ohmic current ramp phase, indicating the accumulation of radiating metallic impurities in the plasma core.

The observed increase in radiation and radiation peaking with  $M_{\text{eff}}$  is correlated with a reduction in the central electron temperature. Given the increase in volume averaged electron temperature with  $M_{\text{eff}}$ , shown in figure 4, this results in a decrease in temperature peaking as  $M_{\text{eff}}$  is increased. This is illustrated in figure 8, where the electron temperature peaking is plotted against bulk plasma radiation. Although the bulk radiation is small compared to the total Ohmic heating power during this period (of the order of 10%), simulations, discussed in the next section, indicate a hollow Ohmic heating profile while the current diffuses into the plasma centre during the current ramp-up phase. Thus, the combination of a peaked radiation profile and a hollow Ohmic heating profile can lead to a significant effect at the plasma centre. Taken together these observations suggest that a key reason for the reduction in electron temperature peaking is cooling of the plasma centre by impurity radiation. Current diffusion modelling, presented in the next section, shows that this systematic variation in electron temperature peaking was the primary cause of the change in the  $q$ -profile evolution during the current ramp phase.

### 3. Current diffusion modelling

Two plasmas from the experimental dataset described in the previous section were simulated to understand the factors

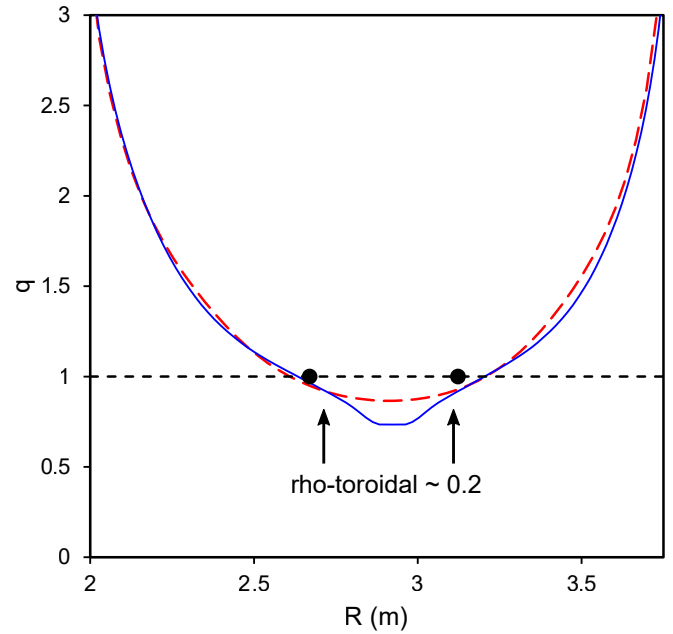


**Figure 9.**  $q$ -profiles from a TRANSP simulation (solid—blue) and EFIT constrained equilibrium reconstruction (broken—red) at  $t = 3.6$  s for a protium plasma. Also shown is the inversion radius of the first sawtooth crash at  $t = 3.63$  s (filled black circles) and the approximate location of  $\rho_{\text{tor}} = 0.2$ .

affecting the  $q$ -profile evolution. The plasmas chosen had the lowest and highest values of main ion isotope mass ( $M_{\text{eff}} \approx 1.10$  and  $1.94$ ), and hereafter they are referred to as the protium (#91263) and deuterium (#91226) plasmas, respectively. The simulations were performed with the TRANSP code [28] using the NCLASS neoclassical resistivity model [29]. The simulations were initiated at the start of the X-point phase using the  $q$ -profile from EFIT constrained by plasma pressure and polarimetry measurements. The electron temperature was provided as spectra from the ECE Michelson interferometer, which were mapped to plasma flux surfaces using the TRANSP equilibrium. The spatial resolution of these measurements is estimated to be 10 cm at the plasma centre, which allows the gross effect of central radiative cooling to be resolved. However, these measurements can smooth out localised features at the plasma edge or very localised cooling in a narrow region close to the magnetic axis. The effective ion charge was provided from the visible bremsstrahlung measurements and assumed to be constant with plasma radius. The plasma density was taken from high resolution Thomson scattering measurements, with the density normalised to match interferometer measurements.

The simulated  $q$ -profile for the protium plasma was compared with the constrained EFIT  $q$ -profile at the time when the first sawtooth crash was observed, as shown in figure 9. The general agreement is good, except in the region  $\rho_{\text{tor}} < 0.2$ , where the strong neoclassical peaking of the electrical conductivity profile is seen in the TRANSP simulation. It cannot be determined whether this feature was present in the experiment as it could not be resolved by the EFIT equilibrium reconstruction due to the limited spatial resolution in the



absence of motional Stark effect data. Both the measured and modelled  $q$ -profiles illustrated in figure 9 are roughly consistent with the location of the sawtooth inversion radius, which is assumed to be close to the  $q = 1$  magnetic surface. It should be noted that  $Z_{\text{eff}}$  was very low in the plasma illustrated in figure 9, and the measurement reached a value of  $\approx 0.9$  at the time of the current ‘overshoot’, which is unphysical. Although this is within the measurement uncertainty, a minimum value of  $Z_{\text{eff}} = 1.05$  was imposed in the TRANSP simulation. This means that the relative difference in  $Z_{\text{eff}}$  between the protium and deuterium simulations is reduced compared with the experimental measurements.

The level of agreement achieved between the modelled  $q$ -profile and experimental data, illustrated in figure 9, contrasts with the previously reported discrepancy between simulated and measured  $q$ -profile evolution in the early current ramp phase of a JET plasma in the presence of a carbon wall [30]. However, there are several key differences to consider: (i) the effective ion charge was much lower during the simulation illustrated in figure 9; (ii) the minimum value of  $q$  was much lower in the simulation illustrated in figure 9, somewhat closer to stationary plasma conditions, where successful modelling was reported in [30]; (iii) electron temperature measurements from the ECE Michelson interferometer were used in the simulation illustrated in figure 9 compared with high resolution Thomson scattering (HRTS) measurements in [30]. Although the spatial resolution is not as high for these ECE measurements compared with the HRTS measurements, the line-of-sight of is much closer to the plasma magnetic axis, which is beneficially for diagnosing the effect of central radiation cooling. Given these analysis differences it is not possible to conclude whether the present level of agreement is in contradiction to the discrepancy previously observed with the carbon wall. Further experiments are required to investigate this point.

Figure 10 shows the time evolution of the  $q$  value at  $\rho_{\text{tor}} = 0.2$  for the protium and deuterium simulations. This radial location was chosen to avoid the central region where the neoclassical feature is evident in the TRANSP simulations. The relative delay in the arrival time of the  $q = 1$  magnetic surface at  $\rho_{\text{tor}} = 0.2$  in the deuterium simulation is qualitatively consistent with the experimental observation in figure 2. As can be seen in figure 10, repeating the protium simulation with the initial  $q$ -profile from the deuterium simulation does not result in any significant change in the arrival time of  $q = 1$  (curve (i)). Repeating the protium simulation with the  $Z_{\text{eff}}$  from the deuterium simulation brings the arrival time of  $q = 1$  even earlier, contrary to the experimental observation (curve (ii)). Repeating this simulation with the electron temperature also multiplied by a time-dependent scale factor so as to match the volume averaged temperature of the deuterium simulation tends to compensate for the  $Z_{\text{eff}}$  change (curve (iii)), resulting in almost no change from the original protium simulation. Repeating the protium simulation with both the  $Z_{\text{eff}}$  value and electron temperature profile from the deuterium simulation (curve (iv)) finally reproduces the  $q = 1$  arrival time of the deuterium simulation. This shows that the reduction in central electron temperature, which reduces the

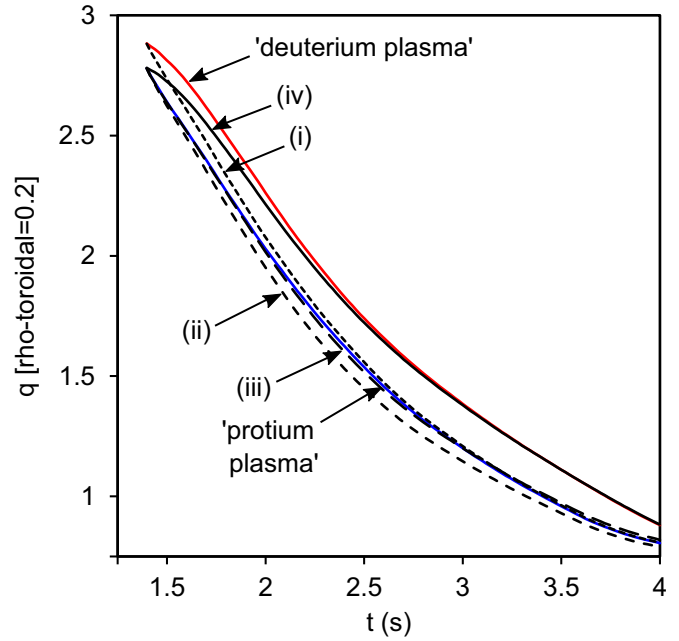


**Figure 10.** Time evolution of  $q$  at  $\rho_{\text{tor}} = 0.2$  from TRANSP modelling for a deuterium plasma (red) and a protium plasma (blue). Protium simulations are also shown with: (i) initial  $q$ -profile from the deuterium simulation; (ii)  $Z_{\text{eff}}$  from the deuterium simulation; (iii)  $Z_{\text{eff}}$  and  $\langle T_e \rangle$  from the deuterium simulation; and (iv)  $Z_{\text{eff}}$  and  $T_e$  profile from the deuterium simulation.

electrical conductivity profile peaking, is the key factor responsible for the change in the  $q$ -profile evolution when the main ion isotope mass was varied in these experiments.

The electron temperature and electrical conductivity profiles used in these simulations are illustrated in figure 11 at  $t = 2.5$  s. The main difference in the electrical conductivity profiles is near the plasma centre, which results in a relatively small change on the plasma internal inductance. For the plasmas illustrated in figure 11, the reduced peaking of the electrical conductivity profile for the deuterium plasma relative to the protium plasma results in a reduction in the internal inductance,  $l_i(3)$ , by  $\sim 4\%$  at the start time of the main heating. It is not expected, therefore, that plasma profile variation of the sort presented in this paper will have a significant impact on transformer flux consumption. It should be noted that the observed increase in radiation peaking as  $M_{\text{eff}}$  was increased could indicate some peaking of the  $Z_{\text{eff}}$  profile. Simulations show that an increase in  $Z_{\text{eff}}$  in the region  $\rho_{\text{toroidal}} < 0.3$  would also reduce the central electrical conductivity, resulting in a further delay in the  $q = 1$  arrival time. This would, therefore, reinforce the effect of the central impurity radiation cooling on the  $q$ -profile evolution.

#### 4. Implication of results for T and mixed D-T operation

A significant fraction of the present JET experiment programme is being devoted to the development of plasma scenarios capable of producing high fusion power in D-T [31]. The aim is to prepare suitable plasma scenarios, as far

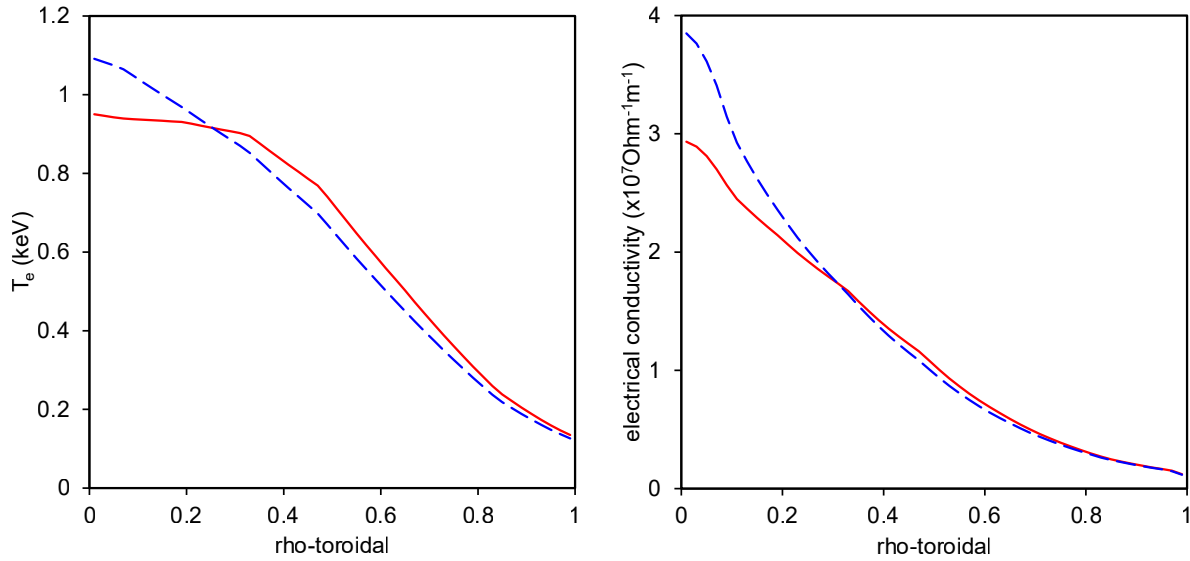


**Figure 11.** Electron temperature profiles (left) and electrical conductivity profiles (right) used for TRANSP simulations illustrated in figure 10. Profiles are illustrated at  $t = 2.5$  s with  $\pm 100$  ms averaging for a deuterium plasma (solid—red) and a protium plasma (broken—blue).

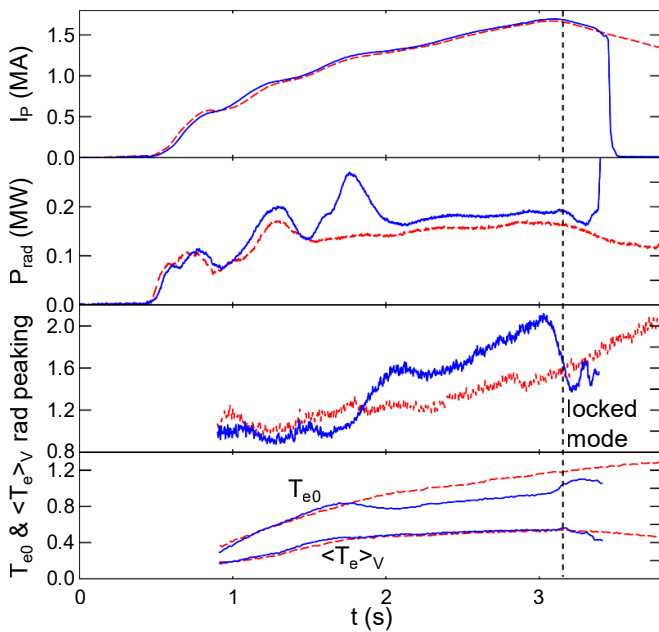


**Figure 12.** Time evolution of plasma current, bulk plasma radiation, plasma radiation peaking and central and volume averaged electron temperature during the initial current ramp phase of two deuterium plasmas. The radiation peaking is characterised as the ratio of the lateral bolometer signal for on-axis channel 14 relative to the average signal from off-axis channels 12 and 16 (see figure 7 for the bolometer lines-of-sight). The onset time for a locked mode is indicated for #89291 (solid—blue). The disruption time can be seen from abrupt drop in plasma current. The comparison pulse is #89289 (broken—red).

as possible, using deuterium. Then it is planned to repeat the deuterium reference plasmas with tritium gas and neutral beam injection to identify any deleterious isotope specific effects and test mitigation strategies before attempting D-T

experiments. In the case of the hybrid scenario it is desirable to reproduce the  $q$ -profile optimised for stability and confinement in deuterium during the subsequent T and D-T experiments. The observed sensitivity of the  $q$ -profile to the main ion isotope mass suggests that, to achieve this, the current ramp phase may need to be modified in T and D-T. For ITB experiments in the 1997 JET-C D-T campaign this was done by modifying the heating power waveform and the start time of the high power heating phase. However, this strategy may not be successful with the JET metallic wall. An investigation performed after the installation of the JET-ILW wall, using current ramp phase representative of hybrid and ITB scenarios, indicated the development of hollow electron temperature profiles due to impurity radiation during the Ohmic ramp phase, unlike comparable experiments with the carbon wall where peaked temperature profiles had been observed [32]. The hollow electron temperature profiles led to magnetic shear reversal and double tearing modes, which had also been seen in Ohmic plasmas in metal wall tokamaks such as FTU due to impurity accumulation [33]. 2/1 modes, typically double tearing, have been observed during the current ramp phase of JET-ILW hybrid plasmas with hollow electron temperature profiles. These modes can lock and then be detected by the real-time protection system, triggering the massive gas injection system to avoid an unmitigated disruption [34]. Although this results in a mitigated disruption, it occurs just after the minimum value of  $q$  in the plasma core falls below 2, which tends to coincide with the current ‘overshoot’, leading to potential for disruptions at high plasma current (possibly above 3 MA) in the hybrid scenarios being developed for D-T operation.

A JET-ILW deuterium hybrid plasma that had a disruption in the Ohmic current ramp phase (pulse #89291), is illustrated in figure 12, together with a comparison plasma without such a disruption (pulse #89289). The main differences between the two pulses were the transformer voltage at plasma initiation

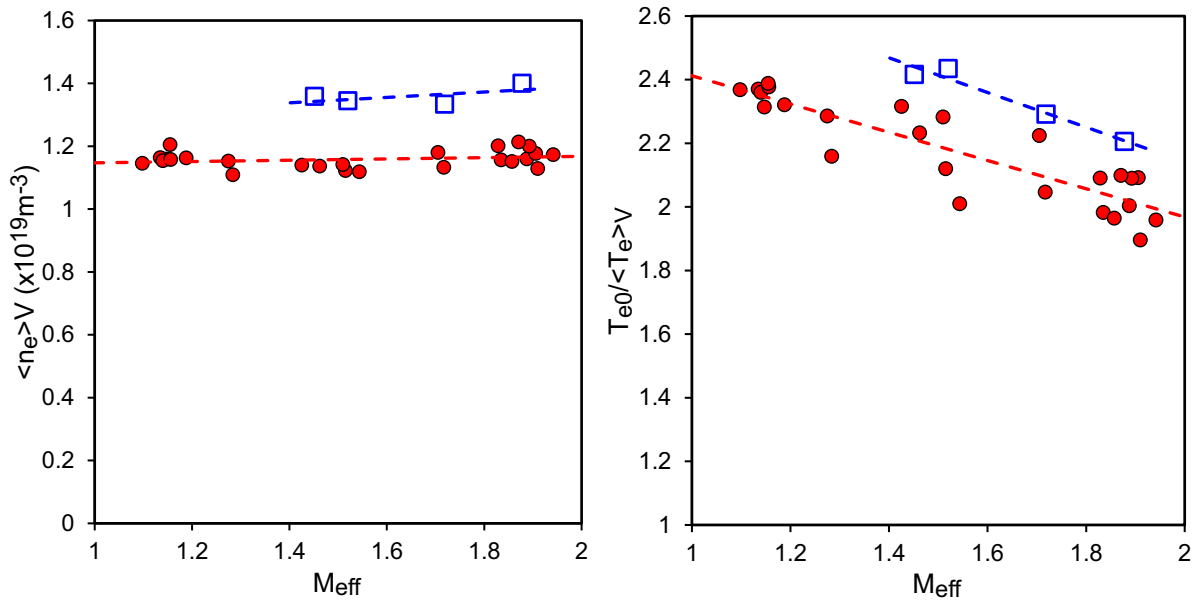


**Figure 13.** Volume averaged electron density measured using high resolution Thomson scattering measurements normalised to match interferometer data (left) and electron temperature peaking (right) plotted against the effective main ion isotope mass. The red filled circles represent the experiments described in the previous section of this paper, and the open blue squares illustrate higher density plasmas. All measurements averaged over  $t = 1.5\text{--}3.5$  s. Linear fits to the data are shown.

and slight changes in the plasma density early in the X-point phase. An increase in radiation early in the X-point phase in #89291 was followed by an increase in radiation peaking compared with #89289. This increase in central radiation was accompanied by a reduction in central electron temperature and electron temperature profile peaking, resulting in a hollow temperature profile. A locked mode then occurred during the current overshoot, which triggered the massive gas injection system and caused a mitigated disruption. The general trend for increased impurity sputtering yield for tritium compared with deuterium [10] suggests an increase in the likelihood of such disruptions due to an increased impurity concentration in T and D-T plasmas, which would occur at high plasma current. This risk cannot be mitigated by modifying the main heating power waveform and/or timing, as in the previous JET-C D-T experiment, as these changes would occur too late to avoid a disruption. Instead, modifications will be required earlier during the current ramp phase to reduce the risk of disruptions.

The measurement of the  $q$ -profile in real-time during the Ohmic ramp phase with sufficient accuracy to resolve core magnetic shear reversal is challenging. However, the strong link between the development of a hollow electron temperature profile and magnetic shear reversal has led to inclusion of an electron temperature profile peaking factor in the JET real-time control system. This will allow several possible control actions to reduce the risk of disruption:

(1) Early pulse termination: In the case where the electron temperature profile becomes excessively hollow in the early current ramp phase, the pulse could be terminated prematurely by rapidly ramping the plasma current down.

This avoids the risk of a high current disruption. In T or D-T experiments it could also minimise the use of tritium and the production of 14 MeV neutrons in pulses that are not matched to the deuterium reference plasmas.

(2) Central heating: In the case of a hollow electron temperature profile, central ICRF heating could be applied to restore temperature peaking, as illustrated in [32]. However, the magnetic field pulse length is limited at high magnetic field in JET, potentially necessitating a magnetic field ramp during the current ramp-up phase on the hybrid scenarios being developed for D-T operation. In this case the ICRF frequencies, that are chosen for on-axis heating during the main heating phase, will not be suitable for on-axis heating early in the current ramp phase.

(3) Density control: Increasing the plasma density during the current ramp phase reduces the plasma electron temperature, allowing more rapid current diffusion and increased temperature peaking. This was noted in [32] and is illustrated for the mixed protium-deuterium experiment in figure 13, where higher density plasmas have been included for which the minimum value of  $q$  at the start of the X-point phase was similar to the values shown in figure 3 and where no abrupt radiation events were observed. In the case of the plasmas shown in figure 13 the increase in plasma density did not reduce the plasma radiation to the low levels observed in the protium plasmas. But the observed increase in temperature profile peaking at higher density suggests that density control by gas puffing might assist in the process of optimising the  $q$ -profile in T and D-T experiments to match the conditions of reference deuterium plasmas. This conclusion is supported by the observation of a strong inverse correlation between the arrival

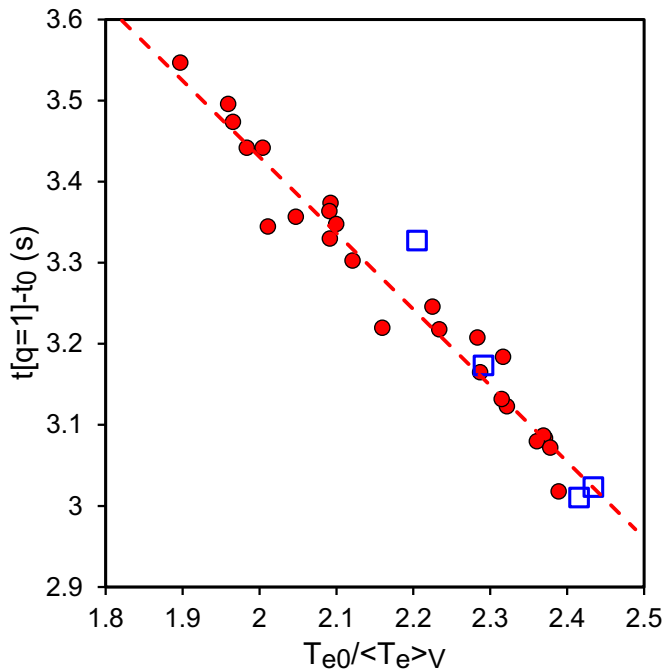


**Figure 14.** Onset time of MHD activity associated with  $q = 1$  relative to the time of plasma initiation plotted against electron temperature peaking averaged over  $t = 1.5\text{--}3.5$  s. The red filled circles represent the experiments described in the previous section of this paper, and the open blue squares illustrate higher density plasmas shown in figure 13. A linear fit to the red symbol data is shown.

time of the  $q = 1$  magnetic surface and the electron temperature peaking, as seen in figure 14. The fact that this inverse correlation holds for both the lower and higher density datasets illustrated in figure 13 shows that a similar  $q = 1$  arrival time can be achieved at different values of  $M_{\text{eff}}$  by varying the plasma density during the Ohmic current ramp phase to match the electron temperature peaking.

A key aim of the deuterium experiments scheduled before the T and D-T campaigns is to establish plasma scenarios capable of sustained high fusion power, including the development of techniques will enable the scenarios that will be optimised for deuterium plasmas to be efficiently transferred to T and D-T.

## 5. Summary and conclusions

It has been shown that increasing the average main ion isotope mass affects  $q$ -profile evolution in the current ramp phase of JET-ILW hybrid plasmas in the presence of the metal wall. The key effect is the decrease in electron temperature peaking as  $M_{\text{eff}}$  is increased, which is consistent with central cooling by impurity radiation. Since the current ramp phase is used to optimise the  $q$ -profile for confinement and MHD stability in JET hybrid plasmas, one can conclude that impurities play a significant role in this process and that the reproducibility of the  $q$ -profile evolution may be sensitive to the condition

of the plasma facing components. The increase in the beryllium sputtering yield for tritium compared with deuterium is markedly smaller than for deuterium compared with protium and only occurs at higher impact energies [10]. Nevertheless, the sputtering of main chamber impurities by charge-exchange neutrals during the X-point phase is expected to increase with tritium leading directly or indirectly to higher plasma radiation. Any increase in impurity confinement with main ion isotope mass would also contribute to the radiation increase. This, in turn, can increase the risk of high plasma current disruptions when hybrid plasmas being developed using deuterium are transferred to T and D-T experiments. Mitigation strategies are being developed using real-time electron temperature peaking measurements to trigger central heating, density control or early pulse termination.

The experience gained from these experiments has relevance to ITER, where initial experiments will be conducted using protium and/or helium before deuterium and mixed D-T operation. Anticipating the effects of isotope changes on plasma behaviour will allow the preparation of any necessary mitigation strategies and ensure effective use of the experience gained in the early phases of operation. The experimental observations and analysis presented in this paper suggest that sophisticated modelling is needed to predict the main ion isotope mass effect on the  $q$ -profile evolution during the current ramp phase in plasma scenarios with low or reversed core magnetic shear. In particular, the integration of plasma wall interactions for impurity sources, scrape-off-layer transport of impurities to the confined plasma, and core impurity transport and radiation, is required for fully self-consistent simulations. This is a challenging task with currently available tools, but the identification of clear trends, such as those presented in this paper, can provide a valuable basis for benchmarking integrated models that can be used to predict the effects in ITER.

## Acknowledgments

The authors wish to acknowledge useful discussions with Pedro Carvalho, Michael Fitzgerald and Anna Widdowson. This work has been carried out within the framework of the EUROfusion Consortium and has received funding from the Euratom research and training programme 2014-2018 and 2019-2020 under Grant Agreement No. 633053 and from the RCUK (Grant Nos. EP/T012250/1). To obtain further information on the data and models underlying this paper please contact PublicationsManager@ukaea.uk. The views and opinions expressed herein do not necessarily reflect those of the European Commission.

## ORCID iDs

S. Brezinsek  <https://orcid.org/0000-0002-7213-3326>  
M. Fontana  <https://orcid.org/0000-0002-7979-7483>  
E. Viezzer  <https://orcid.org/0000-0001-6419-6848>

## References

- [1] ITER Physics Expert Group on Confinement and Transport et al 1999 Chapter 2: Plasma confinement and transport *Nucl. Fusion* **39** 2175
- [2] Gruber O. et al 1999 *Phys. Rev. Lett.* **83** 1787
- [3] Luce T. C. et al 2001 *Nucl. Fusion* **41** 1585
- [4] Hobirk J. et al 2012 *Plasma Phys. Control. Fusion* **54** 095001
- [5] Garzotti L. et al 2019 *Nucl. Fusion* **59** 076037
- [6] Hugill J. and Sheffield J. 1978 *Nucl. Fusion* **18** 15
- [7] Bessenrodt-Weberpals M. et al 1993 *Nucl. Fusion* **33** 1205
- [8] Delabie E. et al 2017 Preliminary interpretation of the isotope effect on energy confinement in Ohmic discharges in JET-ILW 44th EPS Conf. Plasma Physics (Belfast, UK, 26-30 June 2017) P4.159 (<http://ocs.ciemat.es/EPS2017PAP/pdf/P4.159.pdf>)
- [9] Isler R. C., Kasai S., Murray L. E., Saltmarsh M. and Murakami M. 1981 *Phys. Rev. Lett.* **47** 333
- [10] Borodin D. et al 2018 Extrapolation of Be erosion modelling from JET and PISCES-B to ITER. Preprint: 2018 IAEA Fusion Energy Conf. (Gandhinagar, India, 22-27 October 2018) EX/P1-14 (<https://conferences.iaea.org/event/151/contributions/6188>)
- [11] Brezinsek S. et al 2019 *Nucl. Fusion* **59** 096035
- [12] JET Team (prepared by C. Gormezano) 1999 *Nucl. Fusion* **39** 1875
- [13] Challis C. D., Brezinsek S., Coffey I., Hawkes N., Keeling D., King D., Pucella G., Viezzer E. and JET Contributors 2019 Effect of fuel isotope mass on q-profile formation in JET hybrid plasmas 46th EPS Conf. Plasma Physics (Milan, Italy, 8-12 July 2019) pp O2.108 (<http://ocs.ciemat.es/EPS2019PAP/pdf/O2.108.pdf>)
- [14] King D. B. et al 2017 Mixed hydrogen-deuterium plasmas on JET ILW: H-mode confinement and isotope mixture control 44th EPS Conf. Plasma Physics (Belfast, UK, 26-30 June 2017) O3.112 (<http://ocs.ciemat.es/EPS2017PAP/pdf/O3.112.pdf>)
- [15] Sips A. C. C. et al 2009 *Nucl. Fusion* **49** 085015
- [16] Mass A. C. et al 1999 *Fusion Eng. Des.* **47** 247
- [17] Maslov M. et al 2018 *Nucl. Fusion* **58** 076022
- [18] Lao L. L., St. John H., Stambaugh R. D., Kellman A. G. and Pfeiffer W. 1985 *Nucl. Fusion* **25** 1611
- [19] Spitzer L. and Härm R. 1953 *Phys. Rev.* **89** 977
- [20] Schmuck S., Fessey J., Boom J. E., Meneses L., Abreu P., Belonohy E. and Lupelli I. 2016 *Rev. Sci. Instrum.* **87** 093506
- [21] Behringer K. H. et al 1986 *Nucl. Fusion* **26** 751
- [22] Salmon R., Smith P., West A., Shaw S. R., Rendall D. and JET EFDA Contributors 2015 *Fusion Eng. Des.* **98-99** 1148
- [23] Huber A. et al 2007 *Fusion Eng. Des.* **82** 1327
- [24] Widdowson A. et al 2019 *Nucl. Mater. Energy* **19** 218
- [25] Stratton B. C. et al 1989 *Nucl. Fusion* **29** 437
- [26] Behringer K., Denne B., Morgan P. D., Stamp M. and Forrest M. J. 1989 *J. Nucl. Mater.* **162-164** 398
- [27] Marmor E. S., Rice J. E. and Allen S. L. 1980 *Phys. Rev. Lett.* **45** 2025
- [28] Goldston R. J., McCune D. C., Towner H. H., Davis S. L., Hawryluk R. J. and Schmidt G. L. 1981 *J. Comput. Phys.* **43** 61
- [29] Houlberg W. A., Shaing K. C., Hirshman S. P. and Zarnstorff M. C. 1997 *Phys. Plasmas* **4** 3230
- [30] Keeling D. L., Challis C. D., Jenkins I., Hawkes N. C., Lupelli I., Michael C. and de Bock M. F. M. the MAST Team and JET Contributors 2018 *Nucl. Fusion* **58** 016028
- [31] Joffrin E. et al 2019 *Nucl. Fusion* **59** 112021
- [32] Mailloux J. et al 2012 Impact of the JET ITER-like wall on the current ramp up phase and q-profile optimisation for hybrid and advanced scenarios 39th EPS Conf. 16th Int. Congress Plasma Phys. (Stockholm, Sweden, 2-6 July 2012) P4.084 (<http://ocs.ciemat.es/epsicpp2012pap/pdf/P4.084.pdf>)
- [33] Buratti P. et al 1997 *Plasma Phys. Control. Fusion* **39** B383
- [34] Piron L. et al 2019 Experimental and modelling study of locked mode dynamics prior to disruptions in high performance JET plasmas 46th EPS Conf. Plasma Phys. (Milan, Italy, 8-12 July 2019) O4.109 (<http://ocs.ciemat.es/EPS2019PAP/pdf/O4.109.pdf>)